The Astrophysical Journal, 593:370–376, 2003 August 10

EJECTA DETECTION IN MIDDLE-AGED LARGE MAGELLANIC CLOUD SUPERNOVA REMNANTS 0548−70.4 AND 0534−69.9

S. P. Hendrick, K. J. Borkowski, and S. P. Reynolds
Physics Department, North Carolina State University, Raleigh, NC 27606; sphendri@unity.ncsu.edu, kborkow@unity.ncsu.edu, steve_reynolds@ncsu.edu
Received 2002 November 8; accepted 2003 April 18

ABSTRACT

We have observed supernova remnants 0548−70.4 and 0534−69.9 in the Large Magellanic Cloud (LMC) with the *Chandra X-Ray Observatory* and report on the X-ray spectral analysis. Our images of 0548−70.4 and 0534−69.9 show bright central regions as well as brightened limbs. The X-ray spectra from the central regions exhibit enhanced metal abundances, in significant contrast to limb spectra, which show abundances consistent with the LMC interstellar medium (ISM). Considering the relatively old ages (∼10,000 yr), these supernova remnants might be assumed to be in the Sedov phase, in which the X-ray spectra would be dominated by swept-up ISM material. The detection of high abundances in these old remnants is therefore surprising. Spectra from the limb regions were analyzed with Sedov models. The results were then used to account for blast wave emission seen in projection toward the central region and were added to a plane-parallel shock model for the reverse shock in the ejecta. We find elevated levels of iron, oxygen, magnesium, silicon, and sulfur in the bright central regions of each remnant. We introduce a new X-ray spectral shock model appropriate for heavy-element-dominated plasmas, in which electrons liberated by successive ionizations dominate the electron pool and modify the electron temperature profile. With this model, we find reverse-shock speeds of 420 km s^{-1} for 0548−70.4, 500 km s^{-1} for the northeast central region of 0534−69.9, and 360 km s^{-1} for its south central region. The elemental abundances favor a Type Ia supernova origin for both 0548−70.4 and 0534−69.9.

Subject headings: ISM: individual (SNR 0534−69.9, SNR 0548−70.4) — Magellanic Clouds — shock waves — supernova remnants — X-rays: general

On-line material: color figures

1. INTRODUCTION

Supernovae and their remnants (SNRs) are responsible for the synthesis and distribution of heavy elements in the interstellar medium (ISM). Core-collapse supernovae from massive stars (Types Ib, Ic, and II) and detonating white dwarf explosions (Type Ia) produce markedly different proportions of these elements. (See Iwamoto et al. 1999 for a recent summary of several model calculations.) Core-collapse remnants are dominated by oxygen, with predicted O/Fe ratios of the order of 70 (by number), while iron is the main component in Type Ia remnants (O/Fe < 1) (the solar ratio is 18; Anders & Grevesse 1989). We will quote all abundances by number unless otherwise specified.

Since, in both cases, about 10^{51} ergs of energy are released into the ISM, discriminating supernova type from observations of remnants has been a difficult task. However, the combination of spectral and angular resolution of the *Chandra X-Ray Observatory* can aid in the determination of SNR progenitor types, if ejecta emission can be distinguished. This should be possible for very young remnants, but after a few thousand years, the mass of swept-up ISM will greatly exceed the mass of the ejecta, and the remnant will move into the Sedov phase (Sedov 1959). However, this picture is clearly oversimplified, as recent X-ray observations of relatively old SNRs may have revealed evidence for emission from metal-rich ejecta (Maeda et al. 2002; Hughes et al. 2003; Park et al. 2003).

Mature SNRs in the Magellanic Clouds (MCs) with evidence of ejecta are interesting, particularly if X-ray spectral analysis can allow discrimination between core collapse and Type Ia origins. The rates of these two types of explosion are crucial for understanding the chemical evolution of dwarf galaxies such as the MCs. Numerous chemical abundance determinations have revealed a lower O/Fe ratio in the MCs than in Galactic stars of comparable metallicity (i.e., with the comparable Fe/H ratio). While interpretation of this finding is subject to many uncertainties connected with the modeling of MC chemical evolution (Tsujimoto et al. 1995; Pagel & Tautvaišienė 1998), Tsujimoto et al. (1995) suggested an increased frequency of Type Ia versus core-collapse SNe as a partial solution to a low O/Fe abundance ratio in the MCs. Hughes et al. (1995) indeed found a high proportion of Type Ia SNRs in their MC SNR sample observed by the *ASCA* satellite. Systematic studies of evolved MC SNRs with evidence of ejecta by *XMM-Newton* and *Chandra* should allow a more accurate determination of the present-day Type Ia/core-collapse explosion frequency ratio.

The LMC, at a distance of 50 kpc with little extinction, contains over 40 SNRs at different stages of evolution, detailed in radio (Mathewson & Clarke 1973) and X-ray (Williams et al. 1999) surveys. Optical observations of SNR 0548−70.4 show it belongs to the class of Balmer-line dominated, probably Type Ia remnants (Tuohy et al. 1982; Smith et al. 1991; Smith, Raymond, & Laming 1994). Smith et al. (1991) calculate a shock speed of 670 km s^{-1} for this object. SNR 0534−69.9 has been classified by its morphology as a diffuse-face SNR (Williams et al. 1999), but this work is the first to examine this object in detail. Optical emission from radiative shocks has been detected in selected locations within both SNRs (Tuohy et al. 1982; Mathewson et al.

1983; Smith et al. 1991), suggesting that the ambient medium contains denser clumps embedded within a more diffuse ISM. Here we present evidence of substantial ejecta emission in these two middle-aged, Sedov-phase remnants.

2. DATA ANALYSIS

We observed 0548−70.4 (observation ID 1992) on 2001 September 16 for 60.1 ks and 0534−69.9 (observation ID 1991) on 2001 September 1 for 60.2 ks. Both remnants fit entirely on the back-illuminated S3 chip. The data were processed with CIAO 2.2.1 software from the *Chandra* X-Ray Center (CXC). Filtering was performed for good time interval, bad grades, observation-specific bad pixels, and high background times. The processed images of the observations can be found in Figures 1 and 2. Each image has been smoothed with the CIAO tool *csmooth* over a small 2–3 pixel scale to preserve the details of the features. SNR 0548−70.4 has two bright limbs to the east and west, with bright emission in the western part of the interior. SNR 0534−69.9 has a more complex morphology. A bright limb exists in the northwest portion, while the southern limb of the remnant is dim. Two bright features in the central region can be seen in the northeast and south. A detailed analysis of the X-ray spectrum of each region of these remnants is in preparation. We estimate the radii R of these objects to be 12.1 pc for 0548−70.4 and 13.7 pc for 0534−69.9 on the basis of the angular sizes of the X-ray images, assuming a distance of 50 kpc.

Spectra were extracted from each region shown in Figures 1 and 2 and were binned to contain a minimum of 15 counts bin^{-1}. The corresponding response files were created, and the ACISABS model was applied to account for quantum efficiency degradation caused by hydrocarbon contamination. Source-free regions of the S3 chip were used for background subtraction. A comparison of the spectra for the limbs and central regions can be seen in Figures 3, 4, and 5. Here we have included model fits to the central regions that will be discussed later. The most obvious difference is the amount of emission in the 0.5–1.0 keV range, where Fe L-shell lines are important. In Figure 4, the limb emission exceeds the central emission, but the shape of the spectra

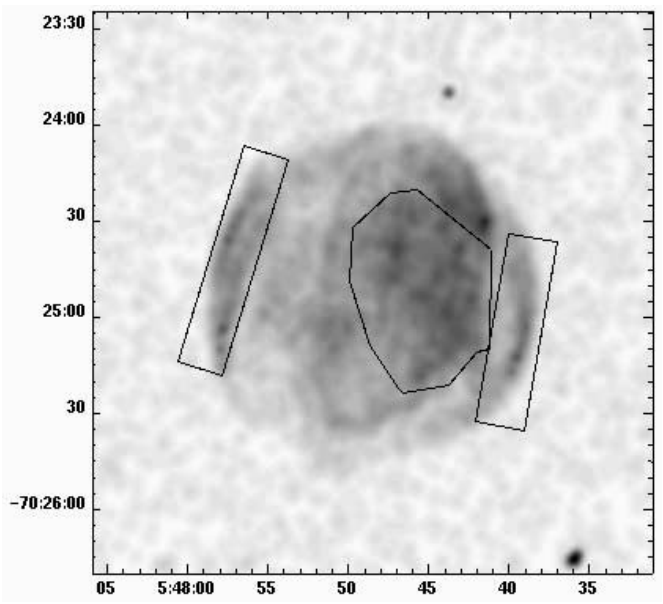

FIG. 1.—Image of SNR 0548−70.4 with 3′ × 3′ field of view. Regions drawn indicate the areas extracted for spectral analysis. [*See the electronic edition of the Journal for a color version of this figure.*]

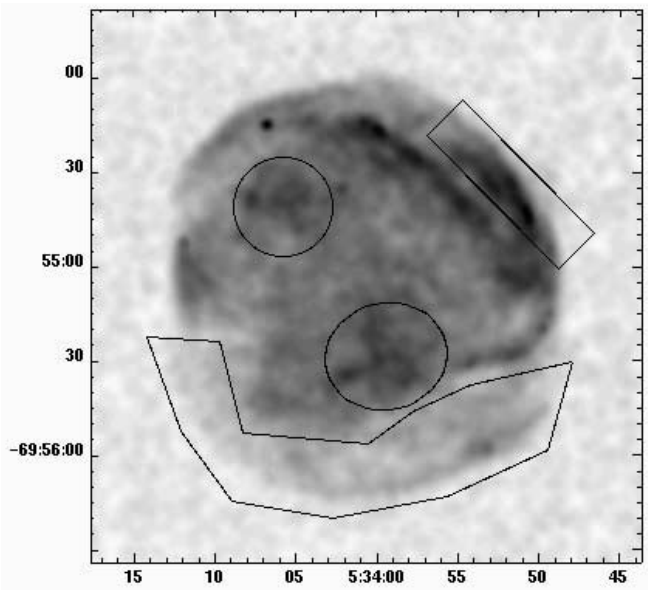

FIG. 2.—Image of SNR 0534−69.9 with 3′ × 3′ field of view. This remnant has a very complicated morphology. [*See the electronic edition of the Journal for a color version of this figure.*]

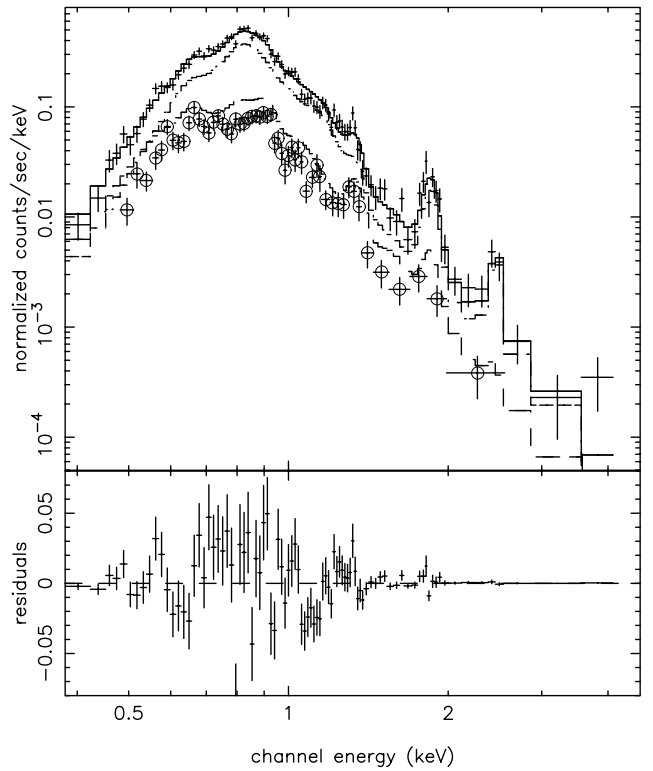

FIG. 3.—Plot of the central region data (*crosses*) and limb region data (*circles*) for 0548−70.4. *Curves*: Upper curve that passes through the central-region data is a two-component fit to those data, and the two lower curves are the two components separately. The lower of the two curves represents the Sedov model component, which matches the limb spectrum in shape, and the upper curve is the *upshock* model that accounts for the Fe L-shell emission and other line emission in the central regions. [*See the electronic edition of the Journal for a color version of this figure.*]

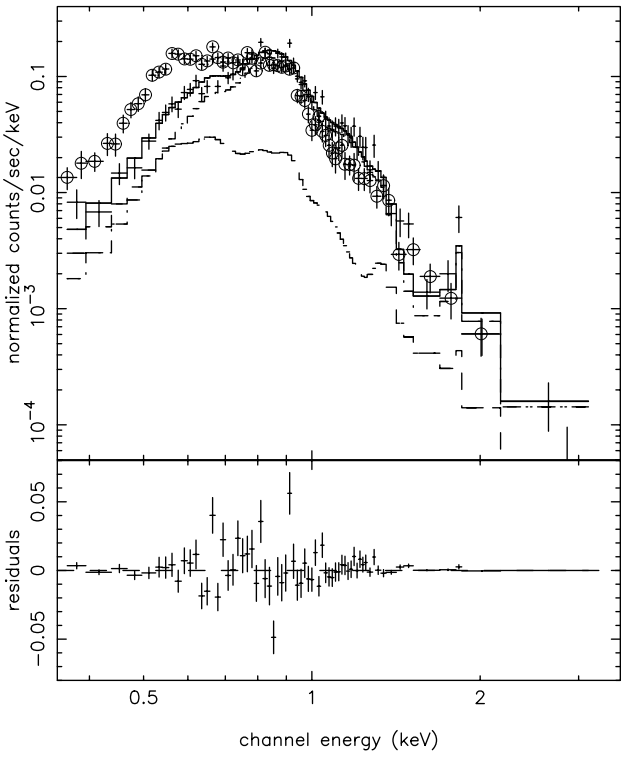

FIG. 4.—Plot of the northeast central region data (*crosses*) and northwest limb region data (*circles*) for 0534−69.9. *Curves*: Same as for Fig. 3. However, in this case, the limb region contained more counts than the central region. Again, the Sedov component of the two-component fit to the central-region data has the same shape as the limb spectrum, while the strong peak of Fe L-shell emission is apparent in the other component. [*See the electronic edition of the Journal for a color version of this figure.*]

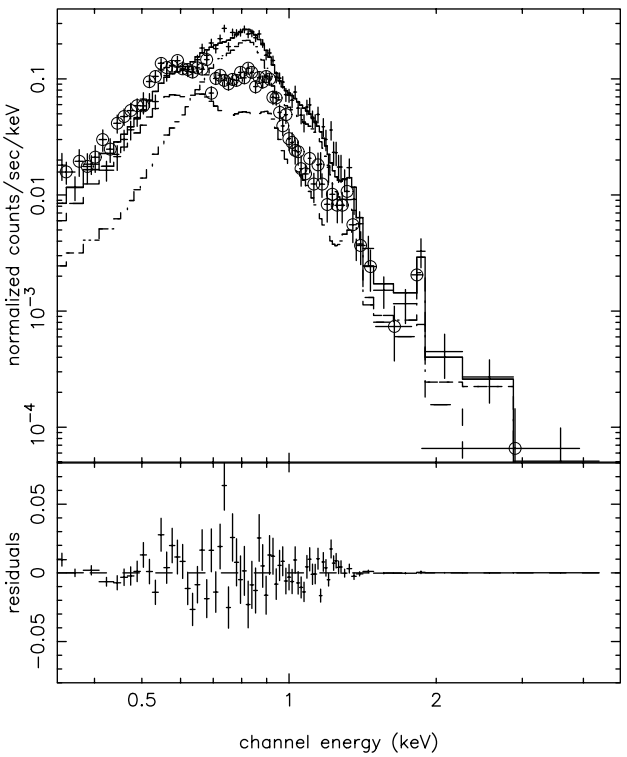

FIG. 5.—Plot of the south central region data (*crosses*) and south limb region data (*circles*) for 0534−69.9. *Curves*: Same as for Fig. 3. [*See the electronic edition of the Journal for a color version of this figure.*]

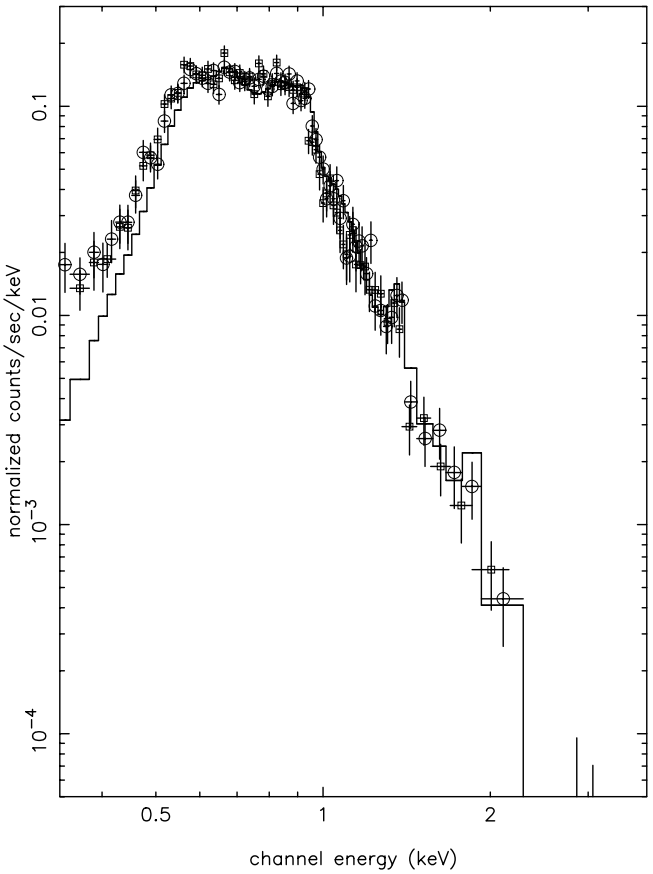

FIG. 6.—CTI-corrected data (*circles*) vs. standard CXC processing data (*squares*) for the northwest limb of 0534−69.9. Notice how the model, which fits the CXC data well, underpredicts emission when applied to the CTI data due to the difference in RMFs at low energies. [*See the electronic edition of the Journal for a color version of this figure.*]

indicates the excess of Fe. Kα emission lines of helium-like Mg, Si, and S also vary in strength across the different regions.

The question of charge transfer inefficiency (CTI) is important when analyzing *Chandra* data. The effects for the back-illuminated S3 chip are much less than the front-illuminated chips. The CIAO software from the CXC cannot account for CTI in the S3 chip, so we have used the PSU CTI corrector (Townsley et al. 2000). Figure 6 compares CTI-corrected data from the northwest limb of 0534−69.9 to uncorrected data. Only slight differences are observed in the position of the data points. The CTI-corrected northwest limb spectrum contains 4556 counts compared to 4395 counts from regular processing. The main difference can be seen in the low-energy regime, when the model (in this case, our best-fit Sedov model to the northwest limb) is applied. Similar differences are seen in each extraction region spectrum when compared to its CTI-corrected spectrum. Plucinsky et al. (2002) compare results of SNR E0102−72.3 data for both the CXC processing and the PSU CTI. There they find agreement in the analysis results using both methods, though fits to the CTI-corrected data resulted in a low absorbing column density that most likely reflects the effect seen in Figure 6. A study of the CTI against Cas A S3 data is available at the CXC web site, where Townsley finds significant improvements in that bright object. For the low signal-to-noise ratio (S/N) in the LMC SNR observations

presented here, any improvements in the data quality are overwhelmed by the photon noise. The underestimate of the data at low energies is due to the difference in the response matrix files (RMF). The gain behavior of the RMFs provided with the corrector are untested in the low-energy (0.2–0.5 keV) range of S3 because calibration information is lacking. Until the question of low energy response can be resolved, we shall continue our investigation of these low S/N remnants without employing any CTI correction for S3 data.

The emission in the limbs is presumably caused by blast wave interaction with the ISM and may be described by a Sedov model. In the presence of ejecta, central emission would be a combination of reverse–shock-heated ejecta and the blast wave emission projected against the center. We attempted to fit a single-component shock model to the central regions, with poor results. However, freeing the Fe abundances from the solar ratios did improve the fits. This was an indication that a single thermal component was too simple a description for the central regions of the remnants. Although the fits were still unacceptable, they did demonstrate enhanced emission from Fe in the centers, which we attribute to ejecta. In order to best describe the central emission, we therefore need to use a two-component model. With the Sedov model fits to the limbs accounting for the blast wave, we can use a plane-parallel shock model (XSPEC model *vpshock*; Arnaud 1996) as the second component to determine the abundances of the ejecta. This model is characterized by an electron temperature, assumed constant, and a maximum ionization timescale $\tau \equiv n_e t$ of the shocked material. All nonequilibrium ionization (NEI) models in XSPEC include modern atomic data for the Fe L-shell complex (Liedahl, Osterheld, & Goldstein 1995). We assume no mixing of blast wave H and He in the ejecta, and we fit for O, Ne, Mg, Si, and S abundances relative to Fe.

We also introduce and test a new model for the ejecta emission. This model calculates the contribution of heavy elements, not only to the line emission, but also to the electron density of the plasma over the ionization timescale history. This model should be useful when the radiating plasma has abundances far from solar values and when hydrogen and helium are not the dominant contributors to the electron density. We calculate the changes in electron temperature over the ionization history of the plasma as successive ionizations release cold electrons, which are subsequently heated by Coulomb collisions with hotter electrons and ions. The parameters for this model are ionization timescale $\tau_{\max} \equiv n_e t$ (with t again the shock age), absolute elemental abundances, and shock speed, which replaces the overall shock temperature parameter used in many models. A detailed description of this model with comparisons with other models is in preparation.

3. RESULTS

3.1. *SNR 0548−70.4*

Table 1 summarizes the results of our model fits to the limb regions. We used abundances of 0.4 solar for the ISM in the LMC, both for the Sedov models and for the X-ray absorption in the LMC. Although solar ratios are not accurate for the LMC (Russell & Dopita 1992), the quality of our data would not allow for fitting of the individual abundances in the limbs. The east limb spectrum contained 1764 counts, and the west limb had 1456 counts between 0.3 and 5.0 keV. The problem with solar ratios in the LMC was highlighted in the initial fits that indicate an overabundance of Ne in the limb regions. The fits were poor in the vicinity of the Ne Kα line at 0.9 keV. In order to improve the fit quality, we refitted the limb spectra with Ne free to obtain the results quoted in the table. Each model included two absorption components, one for the LMC and one for the Galaxy. For the foreground Galactic absorption toward the LMC, we used the hydrogen column density of 7×10^{20} cm^{-2} on the basis of observations of diffuse neutral hydrogen in our Galaxy (Dickey & Lockman 1990). The derived LMC hydrogen column density $N_{\rm H}$ is higher than average for the LMC, particularly for 0548−70.4. Observations of the 21 cm H I line emission in this direction reveal a substantial ($\sim 3 \times 10^{21}$ cm^{-2}) amount of H I in the LMC (Luks & Rohlfs 1992; scaled up by 50% according to Staveley-Smith et al. 2003), and additional absorption may be caused by ionized and/or molecular gas.

For 0548−70.4, Smith et al. (1991) determined a shock speed v_s of 670 km s^{-1} for the east limb material from the observed width of the broad component of the Hα line (assuming no collisionless electron heating at the shock). This shock speed was used to constrain the fit in the east limb, where the optical emission was detected. The fitted values for the west limb are consistent, within errors, with the east limb results. In each Sedov model, the initial electron temperature was essentially zero, with upper limits quoted in Table 1. Those upper limits are lower than the shock temperature values, indicating a lack of equilibration

TABLE 1
SEDOV MODEL FITS TO LIMB REGIONS

	SNR 0548−70.4		SNR 0534−69.9	
PARAMETERS	East Limb	West Limb	Northwest Limb	South Limb
χ^2/dof	63.7/51	69.7/44	91.5/61	83.3/65
$N_{\rm H}/10^{21}$ cm^{-2} (LMC)	$5.22^{+1.1}_{-1.2}$	$3.67^{+1.9}_{-1.1}$	$2.58^{+3.1}_{-0.2}$	$1.90^{+1.6}_{-0.7}$
Abundances (except Ne)	0.4	0.4	0.4	0.4
Ne abundances	$0.55^{+0.15}_{-0.11}$	$0.52^{+0.17}_{-0.15}$	$0.59^{+0.08}_{-0.14}$	$0.68^{+0.12}_{-0.12}$
kT_s (keV)	0.54[a]	$0.79^{+0.96}_{-0.54}$	$0.34^{+0.02}_{-0.19}$	$0.33^{+0.04}_{-0.13}$
kT_e (keV)	$0.0^{+0.2}$	$0.0^{+0.44}$	$0.0^{+0.10}$	$0.0^{+0.13}$
τ (10^{11} cm^{-3} s)	$1.89^{+0.95}_{-0.71}$	$1.89^{+2.41}_{-1.15}$	$2.64^{+2.64}_{-1.10}$	$2.43^{+1.71}_{-0.75}$
(EM/$4\pi d^2$) (10^{10} cm^{-5})	4.37	1.64	5.30	3.52

[a] Frozen to value calculated from Smith et al. 1991 shock speed.

between ions and electrons at the shock front. We derive the shock age from Sedov dynamics by $t = 2R/5v_s = 7100$ yr for 0548−70.4. We calculated densities in two ways, from the emission measure parameter (assuming an emitting volume of 2.2×10^{58} cm^3 in the east limb) and from the relationship between the age and ionization timescales. We approximated the limb volume as the cap of a spherical shell of the radius of the SNR, with thickness and the angular extent of the cap determined from the regions of extraction. For the east limb, we found a thickness of 1.2×10^{18} cm and an angular extent of 90°, which, for a distance of 50 kpc, gives the volume we quote. With an ambient density of 0.18 cm^{-3}, we determine the total mass of the swept-up ISM to be 50 $M_\odot$. Still assuming Sedov dynamics, the explosion energy is $E = (R/1.15)^5 \rho/t^2 = 3.0 \times 10^{50}$ ergs for 0548−70.4. This apparent low explosion energy could be the result of energy going into cosmic-ray acceleration.

Single-component *vpshock* fits to the center of 0548−70.4 with all the abundances linked were poorly constrained. Freeing Fe from the solar ratios but keeping the other abundances linked to one another, we get results and 90% confidence ranges of 0.96 (0.80–1.2) for Fe and 0.52 (0.42–0.72) for the rest of the elements, with $\chi^2/\mathrm{dof} = 165/86$. That is, iron abundance relative to the other heavy elements is roughly twice its solar ratio. This result indicates that there is Fe emission beyond the LMC ISM contribution in the central region, so we will add another model component to account for this excess. The two-component fit results of the central region can be seen in Figure 3. The large central region of 0548−70.4 has 8723 counts. Notice how the Sedov model component in the plot differs in normalization from the limb data, while keeping the same shape. The results of the *vpshock* fit plus the Sedov model component for blast wave emission projected against the center are presented in Table 2. In the central region, we find low ionization timescales and shock temperatures similar to the limb values. Fe, O, Mg, Si, and S emission is prominent. We also allowed neon to be fitted in the central regions, but only a small amount was needed in 0548−70.4. Results using the new heavy-element model agree closely with the *vpshock* values as seen in the table, falling within the 90% confidence ranges quoted. Computational constraints do not allow more detailed error analysis at this time. With the heavy-element model, we determine the speed of the reverse shock to be 420 km s^{-1} for the central region of 0548−70.4.

We expect an O/Fe ratio of 70 (by number) for a 20 $M_\odot$ core-collapse explosion and 0.75 for a Type Ia explosion (Iwamoto et al. 1999). For the central region of SNR 0548−70.4, we find a ratio of 16, much higher than expected for a Type Ia remnant, as the optical data suggest. One explanation could be that O is located in denser ejecta than Fe (Dwarkadas & Chevalier 1998). Particularly strong O lines are expected in deflagration models of Type Ia explosions, with O/Fe emission measure ratios of ~100 (Badenes et al. 2003). However, plane-shock models assume a uniform density for each element, so differences in emission measure are interpreted as differences in abundances. If we interpret the O/Fe values in Table 2 as the ratios of emission measures instead of abundances, there is no problem any more with a high O abundance, allowing us to preserve the interpretation of 0548−70.4 as a Type Ia remnant. Another scenario producing a relatively high O abundance in a Type Ia remnant is that if a substantial amount of shock energy is being transferred to cosmic rays, our estimate of the shock velocity on the basis of the fitted electron temperature is too low and our age estimate too high. Then the apparent O/Fe abundance ratio would increase because not all Fe might have been shocked by the present time. In either case, the O/Fe ratio determined would not be as high as the 70 expected for Type II explosions.

To determine the mass of the ejecta, we examine the upper-limit case in which the filling fraction, f, is equal to 1, and use the emission measure for each element and the volume. The central region was approximated as a sphere of radius 1.8×10^{19} cm, giving a volume of 2.5×10^{58} cm^3. In Table 2, the $\mathrm{EM_{EJ}}$ term is defined as $\int n_e n_i dV$, as is appropriate for a heavy-element dominated shock. In order to calculate the contribution of each element to the emission measure, we can replace n_i with n_{elem}/n_i, where n_{elem} is the ion density of a single element. The ratio of electron to ion density is calculated by the HE shock model, so we can determine the value of n_e from the emission measure and the volume. With $n_e/n_i = 8.3$, we find that n_e is equal to 0.026 cm^{-3}. The electron density relates the emission measure of a single element to its total number N_i, so we can sum the contributions of each to the total mass. Our upper-limit calculation of the central region of 0548−70.4 gives 1.28 $M_\odot$ of ejecta. We have assumed that the ejecta are pure heavy elements with no mixing of hydrogen and helium, though both remnants are old enough to have possibly undergone

TABLE 2
Shock Model Fits to Central Regions

	0548−70.4 C+EL		0534−69.9 NEC+NWL		0534−69.9 SC+SL		
Parameters	*vpshock*	HE Shock	*vpshock*	HE Shock	*vpshock*	HE Shock	Solar Ratios
χ^2/dof	146/83	148/83	116/58	114/58	111/64	109/64	...
$(\mathrm{EM}_L/4\pi d^2)$ $(10^{10}$ cm$^{-5})$	$7.09^{+2.6}_{-2.7}$	6.50	$1.01^{+0.4}_{-0.4}$	1.04	$2.00^{+0.5}_{-0.4}$	2.12	...
kT_e (keV) / v_s (km s^{-1})[a]	$0.62^{+0.04}_{-0.03}$	423	$0.92^{+0.48}_{-0.30}$	501	$0.61^{+0.09}_{-0.10}$	356	...
O/Fe[b]	$20.22^{+6.15}_{-6.04}$	15.6	$5.98^{+2.17}_{-2.07}$	5.96	$2.75^{+3.07}_{-1.75}$	2.79	18.2
Ne/Fe	$0.32^{+0.58}$	0.15	$0^{+0.58}$	0	$0^{+0.32}$	0	2.63
Mg/Fe	$0.18^{+0.09}_{-0.08}$	0.20	$0.16^{+0.10}_{-0.08}$	0.15	$0.18^{+0.09}_{-0.08}$	0.18	0.81
Si/Fe	$0.46^{+0.12}_{-0.12}$	0.44	$0.23^{+0.08}_{-0.10}$	0.22	$0.22^{+0.14}_{-0.14}$	0.22	0.76
S/Fe	$0.66^{+0.33}_{-0.26}$	0.62	$0.18^{+0.26}_{-0.18}$	0.17	$0.51^{+0.46}_{-0.46}$	0.50	0.35
$\tau/10^{11}$ cm^{-3}s	$4.15^{+1.99}_{-1.40}$	2.84	$0.97^{+4.03}_{-0.27}$	1.49	$1.46^{+1.64}_{-0.47}$	2.71	...
$(\mathrm{EM_{EJ}}/4\pi d^2)$ $(10^6$ cm$^{-5})$	$86.2^{+9.20}_{-8.02}$	69.5	$2.84^{+0.24}_{-0.68}$	5.20	$7.00^{+0.67}_{-0.71}$	4.84	...

[a] Shock-speed values listed for the HE shock model, while electron temperature is from the *vpshock* model.
[b] Abundance ratios are by number.

significant mixing. Mixed H and He in the ejecta will increase the inferred electron density and lower the density of the heavy ions for the same observed spectrum. We can estimate how much H and He might be present by comparing the ram pressure ρv^2 of the blast wave to that of the reverse shock using our fitted shock speeds and densities. The difference in ram pressures is 1.7×10^{-9} dyn cm^{-2} in 0548−70.4 (the blast wave pressure being larger). Since we expect approximately uniform pressure in the remnant interior, we attribute the deficit in reverse-shock pressure to our not including H and He and determine the densities of those elements needed for pressure balance. Our pressure calculation for the blast wave is made on the basis of the outermost portion of the shock. Pressure should decrease somewhat moving inward, so these values represent an upper limit to the amount of H and He mixing. The amount of mixing we infer has little effect on the plane-shock fits to the centers, so we can repeat our mass calculations. With maximum mixing, our electron density is now 0.98 cm^{-3}, and our lower limit on ejecta mass (times $f^{1/2}$) becomes 0.41 $M_\odot$ in 0548−70.4.

3.2. *SNR 0534−69.9*

Returning to Table 1, we can see the Sedov model fit results for the limbs of 0534−69.9. The bright northwest limb contains 4395 counts, while the large dim south limb region contains 3912 counts. Mean shock temperatures are 0.33 keV in the south limb and 0.34 keV for the northwest limb. As with the previous remnant, electron temperatures were essentially zero, with upper limits well below the lower limits on the shock temperatures. Repeating the calculations from the assumption of Sedov dynamics, the northwest limb of 0534−69.9 has a shock speed of 530 km s^{-1} and an age of 10,100 yr, with similar values for the south limb. With an ambient density of 0.17 cm^{-3} and emitting volume of 1.0×10^{58} cm^3, we determine the total mass of the swept-up ISM to be 60 $M_\odot$. (We again modeled the limbs as a cap of a spherical shell assuming a distance of 50 kpc, with thickness and angular extent for the northwest limb of 8.3×10^{18} cm and 60° and for the south limb of 1.5×10^{19} cm and 150°.) The explosion energy of 0534−69.9 is 2.6×10^{50} ergs. Again, we find an explosion energy well below the expected 10^{51} ergs.

As with 0548−70.4, the single-component fits to the central regions indicate an overabundance of Fe. The northeast center, with 4071 counts, had elemental abundances (excepting Fe) of 0.79 (0.71–0.87) solar, with Fe equal to 2.3 (2.1–8.0), with $\chi^2/\mathrm{dof} = 125/61$. The south center, with 6063 counts, had elemental abundances of 0.72 (0.45–1.6) with Fe equal to 2.8 (1.9–5.8) with $\chi^2/\mathrm{dof} = 123/67$. Here we infer even higher ratios of Fe to other metals of 3–4. Figures 4 and 5 are the two-component fits to the central regions of 0534−69.9. The northwest limb is the brightest region of the remnant, so its spectrum lies above that of the northeast center, but the shapes of the curves still show excess Fe L-shell emission in the center. The distinction is clearer in Figure 5 for the south center. Table 2 contains the results of the fits. We determined the values of Fe, O, Mg, Si, and S, and found no Ne was necessary for either central region. (The upper limit of Ne is quoted in Table 2.) As before, the results with the heavy-element model fall within the 90% confidence ranges quoted for the *vpshock* fits. The derived reverse-shock speeds are 360 km s^{-1} for the south center of 0534−69.9 and 500 km s^{-1} for its northeast center.

Shock speeds and other inferences obtained from plane-shock fits are uncertain because plane shocks most likely oversimplify the ejecta structure. This is the case for Type Ia remnants, where Dwarkadas & Chevalier (1998) find much denser ejecta near the contact discontinuity than at the reverse shock. For estimated explosion energies and swept-up masses listed above, and assuming 1.4 $M_\odot$ of ejecta with an exponential density profile (Dwarkadas & Chevalier 1998), the reverse shock should have propagated to the center of 0534−69.9 at the age of 7200 yr (6200 yr for 0548−70.4). This might not have happened yet if a substantial amount of energy has been transferred to cosmic rays at the forward shock, causing us to overestimate the ages.

In 0534−69.9, more oxygen was detected in the northeast center (an O/Fe ratio by number of 6.0) than in the south center (2.8). These values are much smaller than expected for a Type II explosion, so our results indicate that a massive-star progenitor for SNR 0534−69.9 is unlikely. We return to our earlier arguments of dense clumps of O, or if a substantial amount of shock energy is being transferred to cosmic rays to explain the discrepancy in our O/Fe ratios compared to Type Ia predictions.

Our upper-limit mass calculations yield 0.46 $M_\odot$ in the south central region, with electron density of 0.045 cm^{-3} and a n_e/n_i ratio of 10.2 and 0.20 $M_\odot$ in the northeast center, with n_e of 0.06 cm^{-3} and a ratio of 8.9. Volume and ram pressure were calculated in the same fashion as before. (We estimate the radii of the south and northeast central regions, again assumed spherical, as 1.2×10^{19} and 9.5×10^{18} cm, respectively.) Since we are looking for an upper limit to H and He mixing, we assume no interactions between the pressures of the central regions. The excesses of blast wave over reverse-shock ram pressure are 4.6×10^{-10} dyn cm^{-2} in the northeast center of 0534−69.9 and 7.4×10^{-10} dyn cm^{-2} in its south center. With maximum mixing, our electron density becomes 0.35 cm^{-3}, giving a lower limit on ejecta mass (times $f^{1/2}$) of 0.09 $M_\odot$ in the south center. The northeast center has a mixed electron density of 0.21 cm^{-3}, implying at least 0.12 $M_\odot$ of ejecta.

4. CONCLUSIONS

Classification of progenitor types from the X-ray spectra of supernova remnants is possible with the current generation of X-ray satellites, though it is surprising that it can be done for remnants with ages approaching 10,000 yr. We infer the presence of material with enhanced metal abundance toward the centers of LMC remnants 0548−70.4 and 0534−69.9, and we propose that both are the results of Type Ia explosions on the basis of observed O/Fe ratios in the centers, much lower than expected for remnants of core-collapse SNe. Ranges of inferred ejecta mass are also consistent with Type Ia progenitors. Because the Balmer-dominated SNR 0548−70.4 is not located near any of the known OB associations in the LMC, Chu & Kennicutt (1988) classified this SNR as belonging to an old stellar population. While SNR 0534−69.9 is located 40 pc (in projection) from the OB association LH 80, its physical association with LH 80 is questionable (Chu & Kennicutt 1988). The location of both SNRs relative to OB associations is again consistent with the Type Ia classification. However, we also find that these are low-energy explosions

with a portion of the expected 10^{51} ergs missing. The missing energy might be going into cosmic-ray acceleration. Testing of our new heavy-element plane-shock model was successful. Its incorporation in XSPEC provides a powerful new tool for analyzing X-ray spectra of SNRs. Our results suggest that ejecta detection is possible for moderately sized, middle-aged remnants in the MCs with the current generation of X-ray telescopes. As the observed sample increases, we expect to find a substantial population of SNRs in MCs with strong ejecta emission.

Support for this work was provided by NASA through *Chandra* grant G01-2075X. We thank Paul Plucinsky for help with planning *Chandra* observations of both remnants. We acknowledge discussions with Carles Badenes about X-ray models of Type Ia remnants.

REFERENCES

Anders, E., & Grevesse, N. 1989, Geochim. Cosmochim. Acta, 53, 197
Arnaud, K. A. 1996, in ASP Conf. Ser. 101, Astronomical Data Analysis and Systems V, ed. G. Jacoby & J. Barnes (San Francisco: ASP), 17
Badenes, C., Bravo, E., Borkowski, K., & Domínguez, I. 2003, ApJ, 593, 358
Chu, Y.-H., & Kennicutt, R. C., Jr. 1988, AJ, 96, 1874
Dickey, J. M., & Lockman, F. J. 1990, ARA&A, 28, 215
Dwarkadas, V. V., & Chevalier, R. A. 1998, ApJ, 497, 807
Hughes, J. P., Ghavamian, P., Rakowski, C. E., & Slane, P. O. 2003, ApJ, 582, L95
Hughes, J. P., et al. 1995, ApJ, 444, L81
Iwamoto, K., et al. 1999, ApJS, 125, 439
Liedahl, D. A., Osterheld, A. L., & Goldstein, W. H. 1995, ApJ, 438, L115
Luks, Th., & Rohlfs, K. 1992, A&A, 263, 41
Maeda, Y., et al. 2002, ApJ, 570, 671
Mathewson, D. S., & Clarke, J. N. 1973, ApJ, 180, 725
Mathewson, D. S., Ford, V. L., Dopita, M. A., Tuohy, I. R., Long, K. S., & Helfand, D. J. 1983, ApJS, 51, 345
Pagel, B. E. J., & Tautvaišienė, G. 1998, MNRAS, 299, 535
Park, S., Hughes, J. P., Slane, P. O., Burrows, D. N., Warren, J. S., Garmire, G. P., & Nousek, J. A. 2003, ApJ, 592, L41
Plucinsky, P., Edgar, R., Virani, S., Townsley, L., & Broos, P. 2002, in ASP Conf. Ser. 262, The High-Energy Universe at Sharp Focus: *Chandra* Science, ed. E. Schlegel & S. Vrtilek (San Francisco: ASP), 391
Russell, S. C., & Dopita, M. A. 1992, ApJ, 384, 508
Sedov, L. I. 1959, Similarity and Dimensional Methods in Mechanics (New York: Academic)
Smith, R. C., Kirshner, R. P., Blair, W. P., & Winkler, P. F. 1991, ApJ, 375, 652
Smith, R. C., Raymond, J. C., & Laming, J. M. 1994, ApJ, 420, 286
Staveley-Smith, L., Kim, S., Calabretta, M. R., Haynes, R. F., & Kesteven, M. J. 2003, MNRAS, 339, 87
Townsley, L., Broos, P., Garmine, G., & Nousek, J. 2000, ApJ, 534, L139
Tsujimoto, T., Nomoto, K., Yoshii, Y., Hashimoto, M., Yanagida, S., & Thielemann, F.-K. 1995, MNRAS, 277, 945
Tuohy, I. R., Dopita, M. A., Mathewson, D. S., Long, K. S., & Helfand, D. J. 1982, ApJ, 261, 473
Williams, R. M., Chu, Y., Dickel, J. R., Petre, R., Smith, R. C., & Tavarez, M. 1999, ApJS, 123, 467